Decreasing the uncertainty of atomic clocks via real-time noise distinguish

Richang Dong (董日昌)[1,2], Jinda Lin (林锦达)[1], Rong Wei (魏 荣)[1,*], Wenli Wang (王文丽)[1], Fan Zou (邹 凡)[1,2], Yuanbo Du (杜远博)[1,2], Tingting Chen (陈婷婷)[1,2], and Yuzhu Wang (王育竹)[1]

[1]*Key Laboratory of Quantum Optics, Shanghai Institute of Optics and Fine Mechanics, Chinese Academy of Sciences, Shanghai 201800, China*

[2]*University of Chinese Academy of Sciences, Beijing 100049, China*

**Corresponding author: weirong@siom.ac.cn*

Received November 1, 2016; accepted January 24, 2017; posted online February 23, 2017

The environmental perturbation on atoms is a key factor restricting the performance of atomic frequency standards, especially in the long-term scale. In this Letter, we perform a real-time noise distinguish (RTND) to an atomic clock to decrease the uncertainty of the atomic clock beyond the level that is attained by the current controlling method. In RTND, the related parameters of the clock are monitored in real time by using the calibrated sensors, and their effects on the clock frequency are calculated. By subtracting the effects from the error signal, the local oscillator is treated as equivalently locked to the unperturbed atomic levels. In order to perform quantitative tests, we engineer time-varying noise much larger than the intrinsic noise in our fountain atomic clock. By using RTND, the influences of the added noises are detected and subtracted precisely from the error signals before feeding back to the reference oscillator. The result shows that the statistical uncertainty of our fountain clock is improved by an order of magnitude to 2×10^{-15}. Besides, the frequency offset introduced by the noise is also corrected, while the systematic uncertainty is unaffected.

OCIS codes: 020.1335, 120.3940.
doi: 10.3788/COL201715.050201.

Atomic clocks have been generally used for timing applications[1–4], precise tests of fundamental symmetries[5,6], searching dark matters[7,8], and quantum information science[9,10]. Cesium fountains have been contributing to International Atomic Time (TAI) as the most accurate primary frequency standards for more than a decade[11,12], and rubidium fountains have been accepted as a secondary standard[1,3]. To date, atomic fountain clocks (AFCs) have achieved a low 1×10^{-16} level of total uncertainties and long-term stability of a low 1×10^{-16} even to the 1×10^{-17} level[1–4]. Optical lattice clocks and ion clocks progress rapidly, and now have achieved lower systematic uncertainty and stability of the 1×10^{-18} level[13–19].

The reference frequency for an atomic clock is expected to be a constant, but actually the ambient perturbations coupled to the clock states drift the clock frequency and destroy the uncertainty and the long-term stability. Several common physical effects, like the blackbody radiation (BBR) effect, the ac Stark effect, the density effect, etc., are the major terms that affect the performance of atomic clocks[14,20,21]. Thus, the uncertainty evaluation is of great significance for precise clocks. Generally, there are three alternative approaches for uncertainty evaluation and improvement: (i) precisely measure the relevant parameters of physical effects and the corresponding frequency-sensitive coefficients with small measuring errors[13,14]. (ii) Adjust the working ambience of the clock to obtain a small frequency-sensitive coefficient. For example, clocks work at a cryogenic temperature to obtain a lower BBR shift[16], AFCs operate at a low density to decrease the collision shift[2,22], and optical lattice clocks exploit well-engineered magic wavelength protocol to cancel the lattice-related Stark shift[10]. (iii) Decrease the ambient perturbations. Precise clocks, such as AFCs and optical clocks, always run in lab well with ambient control. Kinds of active and passive control systems for stabilizing the temperature, magnetic field, light field, etc., are adopted by the devices. Almost every breakthrough of the uncertainty limit stems from a new method for better suppression of environmental perturbations, e.g., an active control of the dc Stark field along the axis of a Sr optical clock is demonstrated to null the dc Stark shift with a 1×10^{-19} uncertainty[14]. Groups are trying to suppress environmental perturbations further for a better uncertainty, while it becomes more and more difficult.

In this Letter, we propose a method based on real-time noise distinguish (RTND) for breaking the uncertainty limit of atomic clocks dominated by ambient perturbations. The idea is implemented as follows: (i) probe environment-related parameters in real time with high-precision sensors when the atomic clock is running, (ii) measure the frequency-sensitive coefficient precisely, and (iii) distinguish and reject the contributions of ambient perturbations from every error signal. The output signal of the clock will be immune to specific perturbations. A proof-of-principle experimental demonstration is fulfilled in an AFC[23,24]. We engineer the magnetic field of the device, which is related to the second-order Zeeman

effect, with the extra noise much larger than the intrinsic noise. At the same time a high-precision sensor is used to monitor and record the fluctuations of the magnetic field. Subtracting the detected environmental noises from the error signals, the deterioration from the analog noises is corrected, which leads to the improvement of clock stability, especially at the long integration time. The demonstrated innovation can be applied to a variety of different physical effects on various atomic clocks to improve the accuracy and stability.

In an atomic clock, high stability is realized by referencing the stable oscillator to a high-quality-factor atomic transition profile, averaging as $\tau^{-1/2}$ or τ^{-1} [25,26]. In a microwave clock operating with the Ramsey sequence, the atomic transition probability is given by $[1+\cos(2\pi\delta\nu T)]/2$. Here, T is the interrogation time, $\delta\nu$ is the normal error signal given by

$$\delta\nu = \nu_{\mathrm{LO}} - \nu_A, \tag{1}$$

where ν_{LO} is the frequency of the local oscillator (LO), and ν_A is the atomic resonance frequency. Actually, ν_A is not constant due to the coupling of the atomic internal states with the ambient electromagnetic fields, even under careful controls, and then,

$$\nu_A = \nu_0 + \sum_{i=1}^{N} \nu_i, \tag{2}$$

where ν_0 is the atomic resonance frequency without environmental perturbations, $\nu_i = f_i(x_i)$ is the frequency shift arising from the ith environment-related physical parameter x_i, and N is the total number of related physical parameters. Substituting Eq. (2) into Eq. (1), we obtain

$$\delta\nu = \nu_{\mathrm{LO}} - \left(\nu_0 + \sum_{i=1}^{N} \nu_i\right). \tag{3}$$

The normal error signal $\delta\nu$ fed back to the LO contains the environmental noise and influences the frequency of the LO, as shown in Fig. 1(a) (red line servo loop). The environmental fluctuation then degrades the clock stability as well as the accuracy. Therefore, the performance of the clock is limited by the environmental noise.

As the blue line in Fig. 1(a) shows, our RTND approach uses a detection system to measure the physical parameter x_i in real time. Considering the experimental case involving M ($\leq N$) measurable physical parameters, with Eq. (3), the frequency error corrected at the end of each closed-loop cycle, as presented in Fig. 1(b), is given by

$$\delta\nu_{\mathrm{RTND}} = (\nu_{\mathrm{LO}} - \nu_0) - \left(\sum_{i=1}^{N} \nu_i - \sum_{j=1}^{M} \nu_j^D\right), \tag{4}$$

where $\nu_i^D = f_i^D(x_i^D)$ is the detected frequency deviation when operating in the RTND condition. With high-precision noise detection, ν_i^D approximately equals ν_i.

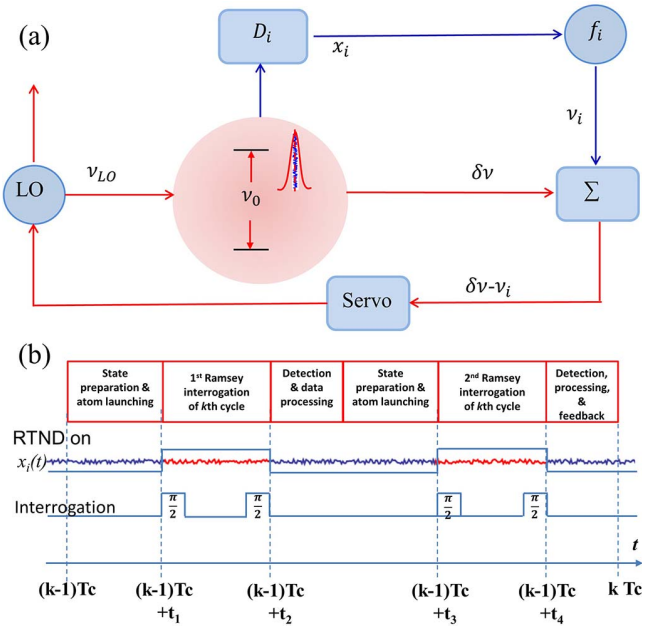

Fig. 1. Principle schematic of the RTND demonstration. (a) The additional sensors group D_i is used to detect the environment-related physical parameters x_i in real time (blue line). The influence of noise on the atomic transition frequency is subtracted from the normal error signal $\delta\nu$ (red line) before being fed back to the LO. (b) The RTND sequence during a closed-loop cycle (Tc). $x_{i,k}(t)$ is the ith environment-related physical parameter during the kth clock cycle. The influential environment fluctuation depicted by the red line in the RTND window perturbs the atomic transition frequency. Its influence is removed from the error signal at the end of the kth cycle.

The RTND approach suppresses the environmental impacts on the clock performance and locks the clock output to noise-immune atomic resonance frequency. In the standard feedback scheme, the total uncertainty $\sigma_0(\tau)$ is deteriorated by environmental noise, and turns out to be

$$\sigma(\tau) = \sqrt{\sigma_0^2(\tau) + \sum_{i=1}^{N} \sigma_i^2(\tau)}, \tag{5}$$

where $\sigma_i(\tau)$ is the uncertainty of ν_i, and the noise sources are independent. The clock stability is ultimately limited by the environmental noise, especially with a long averaging time. With the RTND scheme detecting the ambient fluctuation in real time, the induced frequency errors are eliminated from $\sigma(\tau)$:

$$\sigma_{\mathrm{RTND}}(\tau) = \sqrt{\sigma_0^2(\tau) + \sum_{i=M+1}^{N} \sigma_i^2(\tau)}. \tag{6}$$

As a result, the RTND protocol breaks the uncertainty limit on the normal locking mode.

As we know, the collisional frequency shift plays a crucial role in cooled atomic clocks, e.g., AFCs, and is proportional to the average atomic density $\langle n\rangle$ [27], which can

be detected precisely in real time. Taking into account that $\langle n \rangle = 1.2 \times 10^7$ fluctuating with a standard deviation of 10% and the collisional frequency shift coefficient $k_{\text{coll}} = -5.6 \times 10^{-23}$ cm^3[27,28], the calculated collisional fractional frequency shift of our AFC is -6.7×10^{-16} with an uncertainty of 6.7×10^{-17}. Based on the above theoretical analysis, the collisional frequency shift will be canceled with a decreased uncertainty down to the 1×10^{-18} level by applying the RTND method. This direct improvement can be experimentally demonstrated by a comparison between two high-performance AFCs with a less than 1×10^{-16} level frequency resolution. In our comparison system composed by an AFC and an H-maser, the contribution of the RTND on the collisional frequency shift is hard to distinguish. The noise deterioration method[29], commonly used in this case, is applied to test the RTND scheme.

We experimentally demonstrate the concept of RTND in our ^{87}Rb AFC. The extra noise is added to exaggerate the fluctuation of the corresponding parameter. Specifically, the second-order Zeeman shift is used as the demonstrating effect. The noise, the Allan deviation of which is between the 1×10^{-15} and 1×10^{-14} level, mimics the fluctuation of the atom number of our AFC. The amplitude of noise is set according to the H-maser (VCH 1003A) with the noise floor of about 2×10^{-15}[23], since the demonstration of the RTND is realized by phase comparing the AFC with H-maser. In the normal AFC mode, the noise deteriorates the performance of the frequency output, while in the RTND mode, the noise is detected, and its contribution is canceled.

As shown in Fig. 2, a solenoid surrounding the flight tube is used for supplying the bias magnetic field with a strength of 130.2 nT[30,31]. The subtle fluctuation of the current value is negligible for a clock with the quadratic Zeeman shift of 142.6×10^{-15} and the long-term stability of 1.6×10^{-15}[23]. Then, the noise values are seriatim added to the C-field solenoid for every clock cycle. A precise resistor with a calibrated linearity is used to track the fluctuation of the C-field current. The induced frequency shift is $\nu_B = f_B(B) = k_Z \langle B \rangle^2 = k_C \langle I \rangle^2$, where B is the measured C-field value, k_Z and k_C are the coefficients[30], and $\langle I \rangle$ displays the average C-field current on the cycle. Combining the normally measured error signal $\delta\nu$ and magnetic field induced frequency shift ν_B, the final error is $\delta\nu_{\text{RTND}} = \delta\nu + \nu_B$ with the uncertainty

$$\sigma_{\text{RTND}}(\tau) = \sqrt{\sigma^2(\tau) - \sigma_B^2(\tau)}, \tag{7}$$

where $\sigma_B(\tau)$ is the uncertainty of ν_B.

The fountain clock is running under three different situations: (i) no extra noise for the magnetic field (natural condition); (ii) adding noise to the magnetic field; (iii) RTND correction when noise is added to the magnetic field. To facilitate the description, we substitute the frequency of the AFC for frequency differences between the AFC and H-maser.

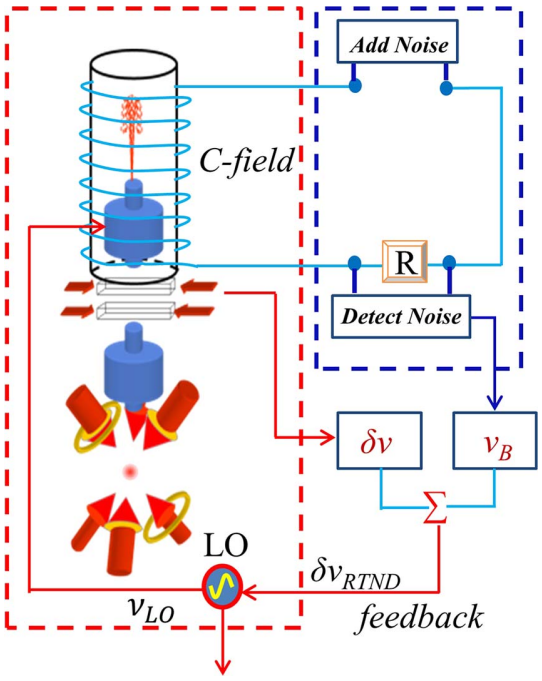

Fig. 2. Experimental diagram of the AFC operating in the RTND protocol. The C-field of the AFC (red line box) is deteriorated by adding noise to the current of the solenoid. A sampling resistor is used to detect the fluctuation of the current, which directly reflects the fluctuation of the magnetic field (blue line box). The influences of the fluctuation are eliminated from the error signal before feedback to the LO.

Frequencies of the three situations are shown in Fig. 3(a). Each data represents the average result of 100 s, and the total measurement time is 150000 s. A group of noises (blue dots) are applied so that the clock's transition frequency is perturbed (red dots). This will decrease the stability in the characteristic averaging time. The amplitude of the frequency fluctuation after the RTND (green dots) is as small as in the natural condition (black dots). Therefore, the frequency fluctuation caused by the magnetic field noise is eliminated. In addition, the frequency offset arising from the noise, shown in Fig. 3(b), is also corrected by the protocol. Here, the black line has an intrinsic frequency difference $(\nu_H - \nu_A)$ between the AFC frequency ν_A and the H-maser frequency ν_H, while the interval between the red line and the black line comes from the noise. In the frequency domain, the histogram of the frequencies under natural conditions is shown in Fig. 3(c) (black histogram). Carrying noises (blue histogram), the frequencies (red histogram) show a wider linewidth than that of natural conditions. When the AFC operates in the RTND condition, the distribution of the clock frequencies (green histogram) is consistent with that under natural conditions. Figure 4 shows that noise with a negative offset of -1×10^{-13} and a positive offset of 0.6×10^{-13} are all corrected by the RTND, leaving the fractional frequency difference coincident with that of a zero offset. In this way, we can compensate the frequency shifts listed in the type-B uncertainty budget using the RTND.

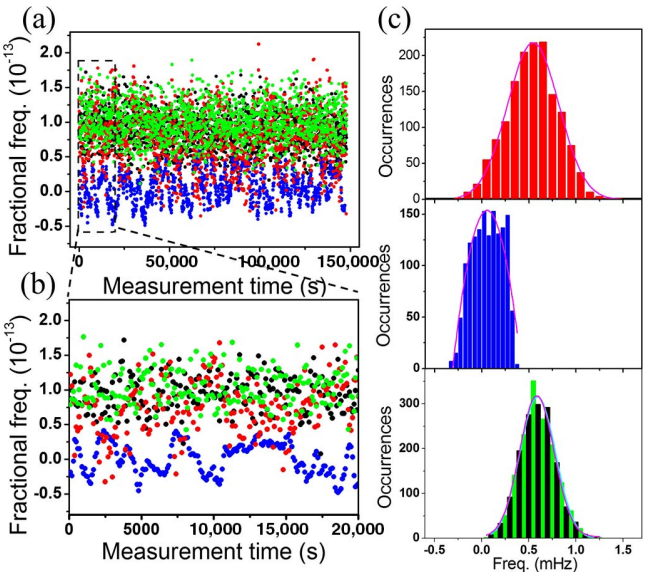

Fig. 3. Frequency differences between the ^{87}Rb AFC and the H-maser. (a) Frequencies for 150000 s at natural conditions (black dots), C-field noise on (red), and RTND on (green). Blue dots denote the frequency shift corresponding to real-time detected C-field noise. (b) Dataset of the frequency difference over a 20000 s interval. (c) Histograms of all of the data corresponding to red, blue, green (black) dots. The linewidth of the green (black) histogram is narrower than the red histogram.

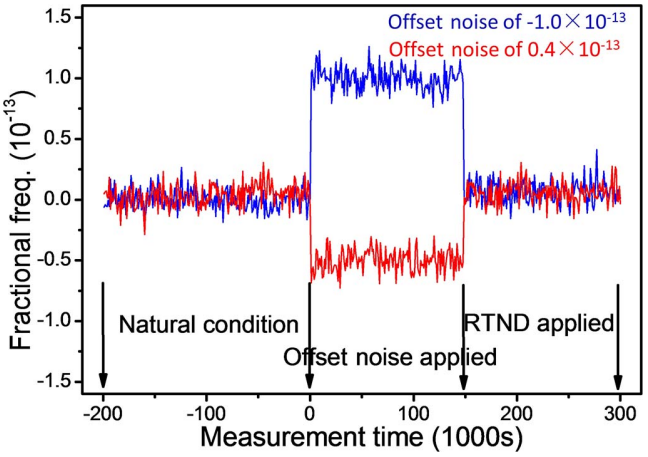

Fig. 4. Illustration of the RTND correction on the offset noise. Noise with a negative offset of -1×10^{-13} (blue line) and a positive offset of 0.6×10^{-13} (red line) are all corrected by the RTND, leaving the fractional frequency difference coincident with that of the zero offset. The intrinsic frequency difference $(\nu_H - \nu_A)$ between the AFC and H-maser frequency in natural conditions has been calibrated to be zero.

To characterize the performance of the RTND in the AFC, we measure the Allan deviation of the frequency fluctuations. Under natural condition, the Allan deviation of the AFC is $2.7 \times 10^{-13}\tau^{-1/2}$ and decreases down to 2.5×10^{-15} for integration time $\tau = 10000$ s, as shown in Fig. 5(a) (black line). The Allan deviation of the extra noise is depicted by the blue line, whose value is between

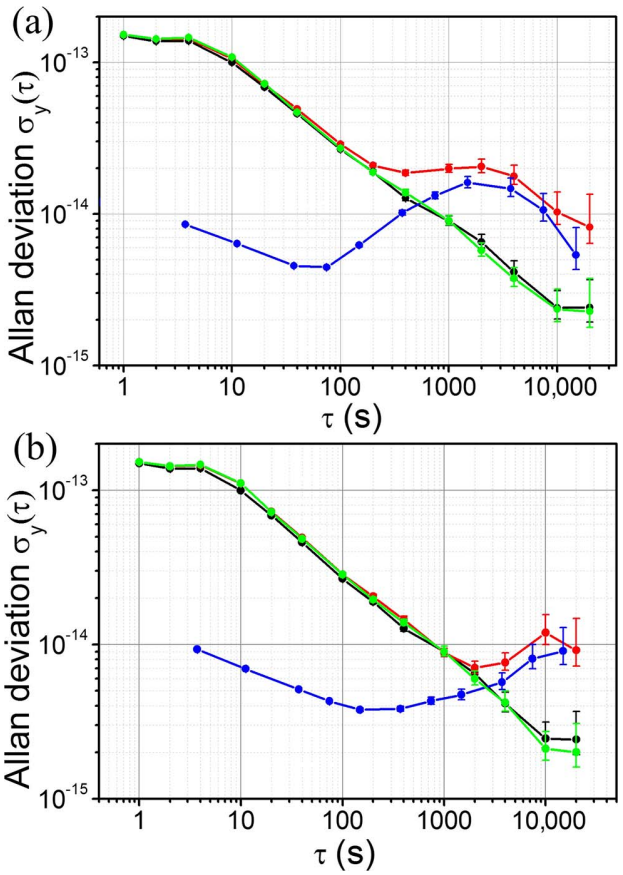

Fig. 5. Normal Allan deviation of the frequency difference when the AFC is running at natural conditions (black), deteriorated by noises (red line), and corrected by the RTND (green line). Blue line: Allan deviation of real-time detected noise. (a) ν_A being deteriorated by a group of experimental noises based on the experimental atom number fluctuations, $\sigma(\tau) = 1 \times 10^{-14}$ (@ 10000 s); after corrected by the RTND, $\sigma(\tau) = 2 \times 10^{-15}$; (b) ν_A being deteriorated by a simulated noise based on Stable32 with the noise parameters 1×10^{-16}, 2×10^{-15}, 2×10^{-14}, 0, and 0 corresponding to random walk of frequency noise (RWFN), flicker frequency noise (FFN), white frequency noise (WFN), flicker phase noise (FPN), and white phase noise (WPN), respectively.

5×10^{-15} and 2×10^{-14}. When the average time is less than 200 s, the instability of the noises is far smaller than the instability of the AFC, and it becomes worse as the averaging time exceeds 500 s. After the noises are applied, the performance of the AFC becomes worse when the averaging time is larger than 200 s (red line). The final result of the Allan deviation follows Eq. (5) in the normal clock locking scheme. After the RTND, the instability of the AFC is reduced (green line), and the result is as good as that under natural conditions (black line), which means that the uncertainty arising from the noises has been eliminated. It is inferred that the RTND method can also effectively suppress some other environmental perturbations on an atomic clock.

To fully test the effectiveness of the RTND, we further engineer time-varying noise by choosing the parameters (Allan deviation at $\tau = 1$ s) of 1×10^{-16}, 2×10^{-15}, and

2×10^{-14} for random walk of frequency noise (RWFN), flicker frequency noise(FFN), and white frequency noise (WFN), respectively, the Allan deviation of the total noise changes with $\tau^{-1/2}$ in the range of 200 s and with $\tau^{1/2}$ after 200 s, as shown in Fig. 5(b) (blue line). When the RTND is applied, the Allan deviation is improved (green line) by approximately one order of magnitude compared to the Allan deviation with noises on (red line) at the averaging time of 10000 s.

In conclusion, we demonstrate an RTND method to decrease the type-B frequency uncertainty and improve the frequency stability of an atomic clock. We apply this method to an AFC with a noisy magnetic field, and the result shows that the stability (@ 10000 s) is improved by approximately an order of magnitude compared to the conventional locking scheme. This technique can significantly ease the requirements on the environmental control ability in an atomic clock. Using the RTND protocol with an accurately calibrated environmental sensor, atomic clocks will break the limit of the control engineering technique on frequency uncertainty and stability. The development of the RTND protocol opens up new directions and possibilities to the improvement of accuracy of other clocks, like the Cs fountain clocks and the Sr optical lattice clocks, by reducing the impact of the collisional shift, the BBR shift, the optical lattice effect, etc.

We thank Professor Bo Yan and Professor Jinming Liu for useful discussions. This work was supported by the National Natural Science Foundation of China under Grant Nos. 61275204 and 91336105.

References

1. J. Guéna, M. Abgrall, A. Clairon, and S. Bize, Metrologia **51**, 108 (2013).
2. T. P. Heavner, E. A. Donley, F. Levi, G. Costanzo, T. E. Parker, J. H. Shirley, N. Ashby, S. Barlow, and S. R. Jefferts, Metrologia **51**, 174 (2014).
3. S. Peil, J. L. Hanssen, T. B. Swanson, J. Taylor, and C. R. Ekstrom, Metrologia **51**, 263 (2014).
4. F. Levi, D. Calonicl, C. E. Calosso, A. Godone, S. Micalizio, and G. A. Costanzo, Metrologia **51**, 270 (2014).
5. X. Zhang, M. Bishof, S. L. Bromley, C. V. Kraus, M. S. Safronova, P. Zoller, A. M. Rey, and J. Ye, Science **345**, 1467 (2014).
6. N. Huntemann, B. Lipphardt, Chr. Tamm, V. Gerginov, S. Weyers, and E. Peik, Phys. Rev. Lett. **113**, 210802 (2014).
7. A. Derevianko and M. Pospelov, Nat. Phys. **10**, 933 (2014).
8. A. Arvanitaki, J. Huang, and K. Van Tilburg, Phys. Rev. D **91**, 015015 (2015).
9. D. J. Wineland, Rev. Mod. Phys. **85**, 1103 (2013).
10. S. Haroche, Rev. Mod. Phys. **85**, 1083 (2013).
11. S. Weyers, U. Hübner, R. Schröder, C. Tamm, and A. Bauch, Metrologia **38**, 343 (2001).
12. C. Vian, P. Rosenbusch, H. Marion, S. Bize, L. Cacciapuoti, S. Zhang, M. Abgrall, D. Chambon, I. Maksimovic, P. Laurent, G. Santarelli, A. Clairon, A. Luiten, M. Tobar, and C. Salomon, IEEE Trans. Instrum. Meas. **54**, 833 (2005).
13. B. J. Bloom, T. L. Nicholson, J. R. Williams, S. L. Campbell, M. Bishof, X. Zhang, W. Zhang, S. L. Bromley, and J. Ye, Nature **506**, 71 (2014).
14. T. L. Nicholson, S. L. Campbell, R. B. Hutson, G. E. Marti, B. J. Bloom, R. L. McNally, W. Zhang, M. D. Barrett, M. S. Safronova, G. F. Strouse, W. L. Tew, and J. Ye, Nat. Commun. **6**, 6896 (2015).
15. N. Hinkley, J. A. Sherman, N. B. Phillips, M. Schioppo, N. D. Lemke, K. Beloy, M. Pizzocaro, C. W. Oates, and A. D. Ludlow, Science **341**, 1215 (2013).
16. I. Ushijima, M. Takamoto, M. Das, T. Ohkubo, and H. Katori, Nat. Photon. **9**, 185 (2015).
17. A. A. Madej, P. Dubé, Z. Zhou, J. E. Bernard, and M. Gertsvolf, Phys. Rev. Lett. **109**, 203002 (2012).
18. K. Beloy, N. Hinkley, N. B. Phillips, J. A. Sherman, M. Schioppo, J. Lehman, A. Feldman, L. M. Hanssen, C. W. Oates, and A. D. Ludlow, Phys. Rev. Lett. **113**, 260801 (2014).
19. C. W. Chou, D. B. Hume, T. Rosenband, and D. J. Wineland, Science **329**, 1630 (2010).
20. E. L. Hazlett, Y. Zhang, R. W. Stites, K. Gibble, and K. M. O'Hara, Phys. Rev. Lett. **110**, 160801 (2013).
21. R. M. Godun, P. B. R. Nisbet-Jones, J. M. Jones, S. A. King, L. A. M. Johnson, H. S. Margolis, K. Szymaniec, S. N. Lea, K. Bongs, and P. Gill, Phys. Rev. Lett. **113**, 210801 (2014).
22. R. X. Li, K. Gibble, and K. Szymaniec, Metrologia **48**, 283 (2011).
23. Y. Du, R. Wei, R. Dong, F. Zou, J. Lin, W. Wang, and Y. Wang, Chin. Opt. Lett. **13**, 091201 (2015).
24. F. Zou, R. Wei, R. Dong, T. Chen, W. Wang, and Y. Wang, Chin. Opt. Lett. **14**, 081201 (2016).
25. G. W. Biedermann, K. Takase, X. Wu, L. Deslauriers, S. Roy, and M. A. Kasevich, Phys. Rev. Lett. **111**, 170802 (2013).
26. M. Meunier, I. Dutta, R. Geiger, C. Guerlin, C. L. Garrido Alzar, and A. Landragin, Phys. Rev. A **90**, 063633 (2014).
27. Y. Sortais, S. Bize, C. Nicolas, A. Clairon, C. Salomon, and C. Williams, Phys. Rev. Lett. **85**, 3117 (2000).
28. C. Fertig and K. Gibble, Phys. Rev. Lett. **85**, 1622 (2000).
29. R. Kohlhaas, A. Bertoldi, E. Cantin, A. Aspect, A. Landragin, and P. Bouyer, Phys. Rev. X **5**, 021011 (2015).
30. R. C. Dong, R. Wei, Y. B. Du, F. Zou, J. D. Lin, and Y. Z. Wang, Appl. Phys. Lett. **106**, 152402 (2015).
31. W. L. Wang, R. C. Dong, R. Wei, J. D. Lin, F. Zou, T. T. Chen, and Y. Z. Wang, Appl. Phys. Lett. **108**, 122401 (2016).